

Time-Domain Analysis for Resonant Beam Charging and Communications With Delay-Divide Demodulation

Mingliang Xiong, Shun Han, Qingwen Liu, *Senior Member, IEEE*, and Shengli Zhou, *Fellow, IEEE*

Abstract—Laser has unique advantages such as abundant spectrum resources and low propagation divergence in wireless charging and wireless communications, compared with radio frequency. Resonant beams, as a kind of intra-cavity laser beams, have been proposed as the carrier of wireless charging and communication, as it has unique features including high power, intrinsic safety, and self-aligned mobility. However, this system has problems such as intra-cavity echo interference and power fluctuation. To study the time-domain behavior of the resonant beam system, we create a simulation algorithm by discretizing the laser rate equations which model the dynamics of the excited atom density in the gain medium and the photon density in the cavity. The simulation results are in good agreement with theoretical calculation. We also propose a delay-divide demodulation method to address the echo interference issue, and use the simulation algorithm to verify its feasibility. The results show that the resonant beam charging and communication system with the proposed demodulator is feasible and performs well. The analysis in this work also helps researchers to deeply understand the behavior of the resonant beam system.

Index Terms—Optical wireless communications, resonant beam communications, resonant beam charging, distributed laser charging, laser communications, 6G.

I. INTRODUCTION

INFORMATION and power are two significant requirements of most mobile electronic devices. These requirements are becoming more and more urgent with the continuing development of new technologies and living standard. For instance, online meeting/class rooms in the future are expected to use virtual reality (VR) or augmented reality (AR) technologies to move the attenders to a metaverse where they can experience face-to-face chat even if they are apart from thousands of kilometers [1–3]. However, the three-dimensional (3D) holographic images/videos transmitted between VR/AR devices have much greater data size than those in two-dimensional (2D) scenario. Moreover, to transmit and process large amount of data, the energy consumption increases dramatically as well. Thus, in the future, the six-th generation (6G) or beyond 6G mobile network is expected to support both information and power transfer [4].

Resonant beam charging and communications systems have been proposed to support simultaneously transferring power and information to remote mobile devices [5–7]. This technology is based on a spatially separated laser resonator (SSLR). Both the transmitter and the receiver are the

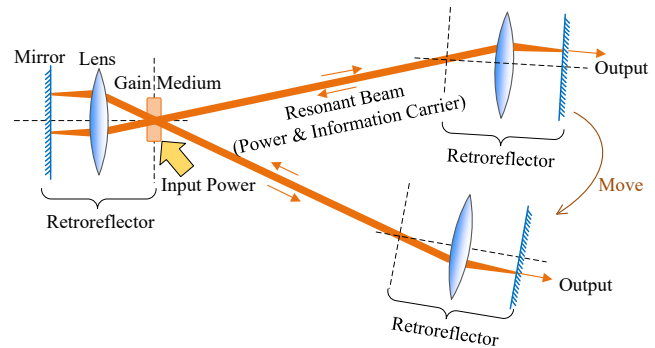


Fig. 1. Mechanism of resonant beam generation

components of the SSLR, different from an integrated laser transmitter. Although integrated laser communication systems have many advantages in spectrum resource, bandwidth, and transmission distance, they still face challenges in some specific scenarios such as indoor mobile communications. Safety and mobility are two important issues in this scenario. As for safety, making a low-power safeguard/detection beam around the high-power laser is one of the protection methods for laser power transfer [8], while it needs accurate positioning/tracking system and sensitive detection system. In terms of mobility, there are many outstanding technologies for fast directing narrow laser beams to remote devices, such as fiber arrays [9], crossed diffraction gratings [10], optical phased arrays (OPAs) [11], and spatial light modulators (SLMs) [12], but the alignment accuracy and the tracking speed also depend on the performance of the receiver positioning technologies [13]. In addition to wireless communications, laser-based wireless power transfer (WPT) also faces challenges in receiver positioning and tracking.

Resonant beam charging and communications based on SSLR can concurrently support intrinsic safety and self-aligned mobility. The primary structure of SSLR originates from Linford’s very long laser proposed in 1973, which consists of two corner cubes and a gain medium [14, 15]. Corner cubes are retroreflectors which reflect beams to their sources. Other retroreflectors such as cat’s eye and telecentric cat’s eye can also be used in the SSLR. As shown in Fig. 1, an SSLR consisting of two telecentric cat’s eye retroreflectors can force photons to oscillate in its cavity even if the position and pose of the retroreflectors are changed; this process generates a light beam connecting the two ends. The gain medium amplifies the beam power, compensating for the power loss that the beam experienced during oscillation. The company Wi-charge discloses a wireless charging system design based

M. Xiong, Q. Liu, and S. Han are with the College of Electronics and Information Engineering, Tongji University, Shanghai 201804, China (e-mail: xiongml@tongji.edu.cn; qliu@tongji.edu.cn; hanshun@tongji.edu.cn).

S. Zhou is with the Department of Electrical and Computer Engineering, University of Connecticut, Storrs, CT 06250, USA (e-mail: shengli.zhou@uconn.edu).

on SSLR (also known as distributed laser cavity), in which two telecentric cat's eye retroreflectors (TCRs) are employed to replace the corner cubes [16]. A focal TCR (FTCR) was proposed in [17]; in this paper, the stable regime of the FTCR-based SSLR was found by theoretical derivation, which is an improvement as the stable regime provides very low diffraction loss within a long moving range. The experiment design of SSLR-based mobile charging in [18] demonstrated charging a smartphone within 2-m distance and 6° field-of-view (FOV) with more than 0.6-W electrical power (received more than 5-W optical power). An experiment on adjustable-free and movable TCR-based SSLR was also demonstrated in [19]. Besides, the safety and mobility of the SSLR were verified by spatial wave-optical simulation [20, 21]. An enhanced experiment on the TCR-based SSLR achieved 5-m transmission distance and 5.91-W received optical power. Moreover, a new SSLR structure based on spatial wavelength division was proposed in [22], which realized 1.7-mW received power at 1-m distance. Besides, capacity analysis of kilometer-level mobile resonant beam communications is presented in [23].

However, there are two significant issues in the resonant beam charging/communication system: the echo interference in modulation and the power fluctuation in movement [24]. These issues affect the efficiency of battery charging and the feasibility of high-capacity communication. A design based on intra-cavity second harmonic generation (SHG) was proposed to avoid the echo interference in the resonant beam communication system [25], while the SHG beam lies in the visible spectrum, which may not be accepted in daily life. Experimentally observing the fast fluctuation of the resonant beam power using an oscilloscope is very expensive, as the frequency band of the echo is much wider than that of the source signal. Time-domain simulation algorithm/program can help reduce the costs of this research, while most related works lack the interest of observing such a micro timescale which is even shorter than the time for a photon to pass through an optical device [26–28]. That's why we have never known what the echo interference looks like. Also, there is no existing method for extracting the source information from the chaotic output directly.

The contributions of this work are as follows:

- 1) We propose a simulation algorithm for the resonant beam charging and communication system to analyze the system behavior in the time domain. We model the dynamics of the excited atoms in the gain medium and the intra-cavity photons by discretizing the rate equations. The simulation algorithm supports observing small-scale power variations, even if the duration is smaller than the time for a photon to pass through the gain medium. We compare the simulation results at the stable state with theoretical computations to verify the high accuracy of the proposed algorithm.
- 2) To overcome the echo interference, we propose a delay-divide demodulation method. This method can directly extract the source information from the chaotic received signal without extra optical devices. Using the simulation algorithm, it is easy to examine the feasibility and the performance of the proposed demodulation method.

Several important scenarios are simulated, such as the start-up of the pump (driving power), the foreign object intrusion/leaving, and the intra-cavity modulation. We also study the demodulator's performance by counting the bit error rate (BER) using the on-off keying modulation.

The remainder of this paper is structured as follows. Section II describes the system model of the resonant beam system, including the static output power model and the dynamic rate equations; it also presents the theoretical foundation of the delay-divide demodulation method. Section III demonstrates the implementation of the simulation algorithm as well as the design of modulation and demodulation. In Section IV, the simulation results are studied, including the responses to the modulation actions and the performance of communication. Finally, conclusions are drawn in Section V.

II. SYSTEM MODEL

Our system design is depicted in Fig. 2. In this section, we first describe the SSLR system. Then, we present the dynamic model of the intra-cavity resonant beam. Finally, we propose the demodulation method which can overcome the effect of the echo interference.

A. System Description

Basically, the SSLR consists of two FTCRs RR1 and RR2 – one at the transmitter and the other at the receiver. Namely, the two ends constitute a resonant cavity. Photons in the cavity oscillate circularly, forming a resonant beam. An external pump source provides the driving power. Generally, the pump source is a diode laser module, if the gain medium is a crystal. There are other kinds of materials that can be used as the gain medium. For example, semiconductors can be pumped by electricity directly. The original photons in the cavity are generated from the spontaneous emission process of the gain medium. As these photons pass through the gain medium in each round trip, their quantity can be increased by the stimulated emission of the gain medium, and this process compensates for their loss induced by the absorption/diffraction of the optical devices. If the input power is sufficient, the optical amplification and the loss will finally reach a balance where the resonant beam can persist. The resonant beam intensity is modulated by an electro-optic modulator (EOM) placed between the mirror M1 and the lens L1 to carry information to the receiver. M2 is a partially reflective mirror, so a portion of the photons can pass through M2 and then be collected for battery charging and information demodulation. The splitter determines how much power to be allocated for charging, and the remainder is for demodulation. The demodulation process contains two low-pass filters (LPFs), an analog-to-digital converter (ADC), a delay unit, and a divider. More details about the demodulation is presented in the next section.

Next, we introduce the stable regime and the output power model of the SSLR. A laser resonator should operate in the stable regime where rays will always oscillate in the cavity and can not escape (geometry optics theory). As a result of this characteristic, stable resonator exhibits extremely low diffraction loss. Generally, spherical-mirror resonators

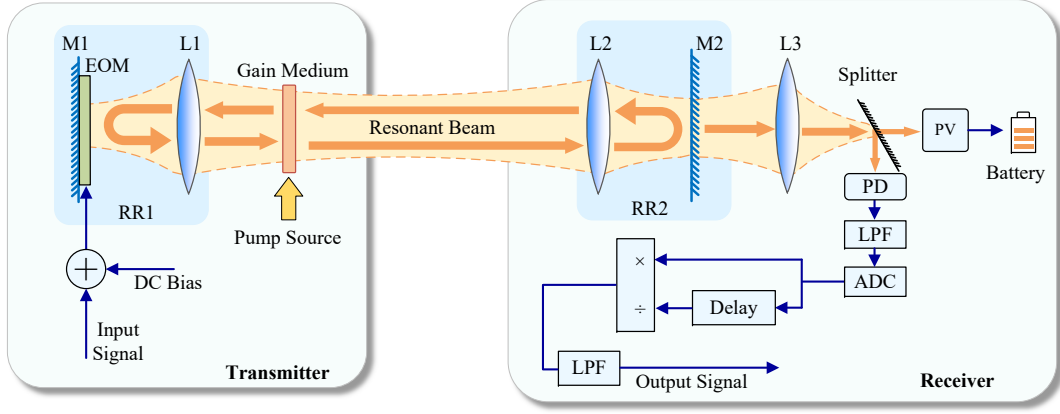


Fig. 2. System design of a resonant beam charging and communications system (M1 and M2: high-reflectivity mirrors; L1–L3: Lenses; EOM: electro-optic modulator for beam intensity modulation; RR1 and RR2: retroreflectors; PV: photovoltaic panel; PD: photon detector; LPF: lowpass filter; ADC: analog-to-digital converter)

with limited cavity lengths are stable. Plane-parallel resonators which consist of two parallel mirrors are not stable, since only the rays perpendicular to the mirrors can be captured by the resonators. In geometry optics, an optical element/system can be described by a ray-transfer matrix [29]. The matrix of a cascaded system is written by the production of the matrices of the components with the reverse order against the input ray's propagation direction. As demonstrated in Fig. 3(a), for an FTCCR, the space interval between the mirror and the lens is l . We set the outer focal plane of the lens as the input/output (IO) plane, namely, the space interval between the lens and the IO plane is equal to the focal length, f , of the lens. The space interval between two IO planes is defined as the transmission distance d . Then, the single-pass ray-transfer matrix of the FTCCR-based SSLR yields [17]

$$\begin{bmatrix} A & B \\ C & D \end{bmatrix} = \begin{bmatrix} 1 & 0 \\ 0 & 1 \end{bmatrix} \begin{bmatrix} 1 & l \\ 0 & 1 \end{bmatrix} \begin{bmatrix} 1 & 0 \\ -1/f & 1 \end{bmatrix} \begin{bmatrix} 1 & 2f+d \\ 0 & 1 \end{bmatrix} \begin{bmatrix} 1 & 0 \\ -1/f & 1 \end{bmatrix} \begin{bmatrix} 1 & l \\ 0 & 1 \end{bmatrix} \begin{bmatrix} 1 & 0 \\ 0 & 1 \end{bmatrix}. \quad (1)$$

By calculation, the elements of the ABCD matrix in (1) are obtained as follows:

$$\begin{cases} A = -1 - \frac{d}{f} + \frac{dl}{f^2}, \\ B = 2f - 2l + d - \frac{2dl}{f} + \frac{dl^2}{f^2}, \\ C = \frac{d}{f^2}, \\ D = -1 - \frac{d}{f} + \frac{dl}{f^2}. \end{cases} \quad (2)$$

Let $g_1^* = A$, $g_2^* = D$, a stable SSLR should satisfy the condition $0 < g_1^* g_2^* < 1$. For such a symmetric SSLR, the up boundary of the transmission distance can be obtained from this stable condition; that is $d < 4f_{RR}$. The intra-cavity resonant beam consists of two parts – the leftward-traveling wave and the rightward-traveling wave. Generally, there are multiple transverse modes in the resonant beam if the devices

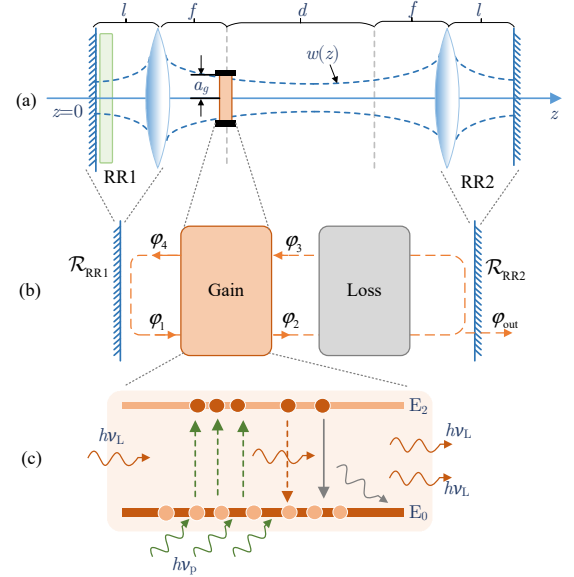


Fig. 3. Diagram of the cavity and the gain medium: (a) cavity structure and beam radius along the optical axis z ; (b) photon circulation in the cavity; and (c) mechanism of optical amplification provided by the gain medium

apertures are much bigger than the radius of the fundamental mode TEM_{00} . The mode radius of TEM_{00} is obtained as [30]

$$w_{00}(z) = \sqrt{-\frac{\lambda}{\pi \Im[1/q(z)]}}, \quad (3)$$

where λ is the wavelength of the resonant beam, $\Im[\cdot]$ takes the imaginary part of a complex number. The $q(z)$ -parameter

is obtained as [17]

$$q(z) = \begin{cases} j|L^*| \sqrt{\frac{g_2^*}{g_1^*(1-g_1^*g_2^*)}} + z, & z \in [0, z_{L1}], \\ \frac{q(z_{L1})}{-q(z_{L1})/f_1 + 1} + (z - z_{L1}), & z \in (z_{L1}, z_{L2}], \\ \frac{q(z_{L2})}{-q(z_{L2})/f_2 + 1} + (z - z_{L2}), & z \in (z_{L2}, z_{M2}], \end{cases} \quad (4)$$

where $j = \sqrt{-1}$; $L^* = B$; and z_{M1} , z_{L1} , z_{L2} , and z_{M2} are the location of M1, L1, L2, and M2, respectively. The ratio of the resonant beam radius to the TEM₀₀ mode radius is a constant at any location on the z -axis. This ratio is called the beam propagation factor. The beam radius is determined by the smallest aperture in the SSLR. Generally, the gain medium has the smallest aperture. Hence, the radius of the resonant beam at location z is obtained as [30]

$$w(z) = \frac{a_g}{w_{00}(z_g)} \sqrt{-\frac{\lambda}{\pi \Im[1/q(z)]}}, \quad (5)$$

where a_g is the radius of the gain medium aperture, and z_g is the location of the gain medium.

Below are loss factors in the SSLR, and they attenuate the circulating power in the cavity. M2 has a partially-reflectivity coating. The reflectivity of M2 is denoted by R_{M2} . Thus, a portion of the rightward-traveling beam is allowed passing through M2. The transmissivities of lenses L1 and L2 are denoted by Γ_{L1} and Γ_{L2} , respectively; namely, a little beam power in the cavity is eliminated by the lenses. Here, M1 and the EOM can be combined as a reflective EOM, as M1 can be considered as a reflectivity coating attached to the EOM. We use $R_{M1,EOM}$ to denote the reflectivity of this reflective EOM. Besides, the gain medium also has absorption/reflection. Therefore, we use Γ_g to represent its transmissivity. The air transmissivity is represented as Γ_{air} . Furthermore, diffraction loss denoted by Γ_{diff} exists in the cavity. To calculate the output power, the SSLR is equivalent to a classical resonator which consists of a gain medium and two mirrors placed on the left and the right sides of the gain medium. The reflectivities of the equivalent mirrors are $\mathcal{R}_1 = R_{M1,EOM}\Gamma_{L1}^2\Gamma_{diff}\Gamma_g^2$ and $\mathcal{R}_2 = \Gamma_{air}^2\Gamma_{L2}^2R_{M2}$, which count the loss factors on the left side and the right of the gain medium of the SSLR, respectively. Then, the output power by M2 can be obtained as [17]

$$P_{out} = \Gamma_{M2}\Gamma_{L2}\Gamma_{air}\eta_{slop} [P_{in} - P_{th}], \quad (6)$$

where

$$\eta_{slop} = \frac{\eta_c}{(1 + \sqrt{\mathcal{R}_2})(1 - \sqrt{\mathcal{R}_1\mathcal{R}_2})}, \quad (7)$$

and

$$P_{th} = \frac{\pi a_g^2 I_s}{\eta_c} \ln \frac{1}{\sqrt{\mathcal{R}_1\mathcal{R}_2}}, \quad (8)$$

where I_s is the saturation intensity of the gain medium, and η_c is the combined efficiency in the pumping process. Note that the loss factors Γ_g and Γ_{diff} appear in the whole body of the gain medium, while for simplicity, we assemble these

factors in the equivalent reflectivity \mathcal{R}_1 . For most transmission distances, these losses are very low and therefore exhibit little effect on the result. If the diffraction loss is high, the results may deviate, but its trend remains the same as the distance increases. The pump laser is generated by a laser diode and then absorbed by the gain medium. The efficiency from electricity to the absorbed power contains the pump diode's electro-optical conversion efficiency η_p , the pump laser transmission efficiency η_t , and the absorption efficiency η_a . With respect to the internal action of the gain medium, there exist the quantum efficiency η_Q , the Stokes factor η_S , and the overlap efficiency η_B . Thus, the combined efficiency is expressed as

$$\eta_c = \eta_B\eta_S\eta_Q\eta_a\eta_t\eta_p. \quad (9)$$

B. Dynamic of Intra-cavity Resonant Beam

As demonstrated in Fig. 3(b), the photons travel back and forth circularly between two retroreflectors. During the circulation, the photons experience the optical amplification provided by the gain medium and also the attenuation induced by many loss factors. However, this process may bring instability to the resonant beam power. There are two aspects that affect the stability of the resonant beam power: the gain fluctuation and the loss fluctuation [7]. The absorption/reflection of lenses and the air as well as the transmission of mirrors can be static or dynamic. For example, if the receiver is moving, the counted reflectivity to the beam at each lens will change with respect to the incident angle. Besides, the EOM can be considered as a dynamic loss if intensity modulation is applied to the resonant beam. The intensity fluctuation also affects the gain medium, leading to the dynamic gain. Hence, we need to model the dynamic process of the resonant beam system and then create a simulation algorithm to observe the fluctuation of the beam intensity, especially when the beam is modulated. As a result of the existence of the echo signal, the past signal is involved in modulation, and therefore, the output signal exhibits a chaos. Generally, it is difficult to demodulate such a chaotic signal. We do the time-domain simulation to find out a method for extracting information from such a chaotic output.

We first study the dynamic behavior of the gain medium. As depicted in Fig. 3(c), the atoms in the gain medium stay at different energy levels. For a four-level gain medium, such as Nd:YVO₄ crystal, the active levels from low energy to high energy are denoted by E_0 , E_1 , E_2 , and E_3 , respectively. When the gain medium is irradiated by the pump laser with frequency ν_p , atoms at E_0 transit to E_3 , and then, quickly transit to a lower stable energy level E_2 . There are two approaches for the excited atoms to transit from E_2 to E_1 , namely, by spontaneous emission or by stimulated emission. Both of the above approaches emit photons with frequency ν_L . If there is no external photon with frequency ν_L passing through the gain medium, the excited atoms at E_2 will transit to lower energy levels spontaneously and meanwhile generate omnidirectional photons. This fluorescence decay operates with a slow rate, for example, the fluorescence time τ_f of Nd:YVO₄ is 100 μ s. However, if the excited atom is stimulated by an input photon with frequency ν_L , it will transit to E_1 rapidly while generating

an identical photon that has the same frequency and direction with the input one. Since the transitions $E_3 \rightarrow E_2$ and $E_1 \rightarrow E_0$ are very fast and nonradiative, few atoms remain at E_3 and E_1 . Thus, we usually simplify the four-level system to a two-level system, as depicted in Fig. 3(c).

The above dynamic process can be expressed by the following rate equations [31]:

$$\frac{\partial N_2}{\partial t} = -N_2\varphi\sigma c - \frac{N_2}{\tau_f} + R_p, \quad (10)$$

$$\frac{\partial \varphi}{\partial t} = N_2\varphi\sigma c - \frac{\varphi}{\tau_c} + S, \quad (11)$$

where N_2 is the atom density at E_2 ; φ is the photon density in the cavity; σ is the stimulated emission cross section of the gain medium; c is the light speed; τ_f is the fluorescence time; R_p is the pump rate; τ_c is the decay time of the intra-cavity photons; and S is the rate at which spontaneous emission contributes to the stimulated emission. The pump rate and the spontaneous emission coupling rate are as follows:

$$R_p = \frac{\eta_c P_{\text{in}}}{h\nu_L V}, \quad \text{and} \quad S = \beta \frac{N_2}{\tau_{21}}, \quad (12)$$

where h is the Planck's constant, $\nu_L = c/\lambda$ is the photon frequency of the resonant beam, V is the volume of the gain medium; β is the spontaneous emission factor that represents the ratio of the spontaneous photons coupled into the laser resonator to the total generated spontaneous photons [32]; and τ_{21} is the decay time of the transition $E_2 \rightarrow E_1$. Generally, β is a very small number (e.g., in this paper $\beta = 0.1\%$). For computer simulation, the rate equations in (10) and (11) can be rewritten into the following discrete form:

$$\Delta N_2 = \left(-N_2\varphi\sigma c - \frac{N_2}{\tau_f} + R_p\right)\Delta t, \quad (13)$$

$$\Delta \varphi = \left(N_2\varphi\sigma c - \frac{\varphi}{\tau_c} + S\right)\Delta t, \quad (14)$$

where Δt represents the unit time in simulation; and ΔN_2 and $\Delta \varphi$ are the variation of the excited atom density and the photon density per unit time, respectively. Every term in the equations represents a physical process. For instance, $-N_2\varphi\sigma c$ describes the stimulated emission rate, $-N_2/\tau_f$ is the decay rate of the excited atom density induced by spontaneous emission, R_p is the increase rate of excited atom density produced by pumping process, and φ/τ_c is the decay rate of intra-cavity photon density induced by cavity loss.

However, the above rate equations describe the behavior of the average densities of the atoms and the photons and do not consider the fluctuation of these quantities within an oscillating period. Since the modulation period can be much shorter than the oscillating period, a micro perspective to the photon density variation is required. Here we set $\Delta t = l_g/c$, where l_g denotes the gain medium thickness. This means that a unit time of simulation is the time for the light to pass through the gain medium. As depicted in Fig. 3(b), the densities of the rightward-traveling photons at the input and the output surfaces of the gain medium are φ_1 and φ_2 , respectively. The densities of the leftward-traveling photons at the input and the output surfaces of the gain medium are φ_3 and φ_4 ,

respectively. Then, from (13), the density of the excited atoms is modeled as the following recursion formula:

$$N_2[n+1] = N_2[n] - N_2[n] \{\varphi_1[n] + \varphi_3[n]\} \sigma l_g - \frac{N_2 l_g}{\tau_f c} + \frac{R_p l_g}{c}, \quad (15)$$

where n is the time index. Equation (15) describes that the current atom density is derived from that before a time step. Similarly, the photon density can also be calculated by summing up the changes within a unit time. Here, we consider the photon densities at the two propagation directions. Then, we calculate the densities of the photons outputting from the gain medium by

$$\varphi_2[n+1] = \varphi_1[n] + N_2[n]\varphi_1[n]\sigma l_g + \frac{S[n]l_g}{2c}, \quad (16)$$

$$\varphi_4[n+1] = \varphi_3[n] + N_2[n]\varphi_3[n]\sigma l_g + \frac{S[n]l_g}{2c}. \quad (17)$$

From (16) and (17), we can see that the output photon densities from the gain medium are derived from the input photon densities. To complete the circulation, we build the relation between φ_1 and φ_4 , and also the relation between φ_3 and φ_2 ; they are

$$\varphi_1[n] = \Gamma_g^2 \Gamma_{\text{diff}} \Gamma_{L1}^2 R_{M1, \text{EOM}} s[n - n_L] \varphi_4[n - 2n_L], \quad (18)$$

$$\varphi_3[n] = \Gamma_{\text{air}}^2 \Gamma_{L2}^2 R_{M2} \varphi_2[n - 2n_R], \quad (19)$$

where $s[n]$ represents the modulation signal; and n_L and n_R are the time steps for the photons to transit from the gain medium to M1 and M2, respectively. Note that the time step of passing the gain medium is 1, which should be considered in the subsequent analysis. The initial condition for the above equations is $\{N_2, \varphi_1, \varphi_2, \varphi_3, \varphi_4\} = 0$.

C. Modulation and Demodulation

The information is modulated on the resonant beam by the EOM. Under this circumstance, we only consider using intensity modulation and direct detection (IM/DD) scheme [33]. In this case, the EOM can be assumed as a multiplier, where the multiplier and the multiplicand are the input resonant beam intensity and the EOM's control signal, respectively. The EOM's control signal should be at least kept above a specific direct-current (DC) level so that enough power is allowed to pass through the EOM to maintain the resonance. Therefore, given the source signal series $x[n]$ and the DC bias $p \in [0, 1]$, the control signal is expressed as

$$s[n] = (1-p)x[n] + p, \quad (20)$$

where $(1-p)$ represents the signal amplitude, which ensures that the control signal is restricted within the range of $[0, 1]$. The beam power is counted as the total energy that passes the beam cross section within a unit time. As a photon with frequency ν_L has the energy of $h\nu_L$, and the beam cross section at the gain medium is approximate to be the cross section of the gain medium, the rightward-traveling beam power at the right-hand side of the gain medium yields

$$P_2[n] = \pi a_g^2 c h \nu_L \varphi_2[n]. \quad (21)$$

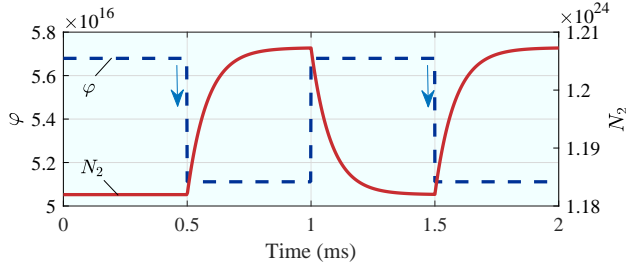


Fig. 4. Response of the excited atom density to the change of photon density

Then, the output power P_{out} is obtained from P_2 by multiplying several loss factors; that is

$$P_{\text{out}}[n] = \Gamma_{\text{M2}}\Gamma_{\text{L2}}\Gamma_{\text{air}}P_2[n - n_{\text{R}}], \quad (22)$$

where $\Gamma_{\text{M2}} = 1 - R_{\text{M2}}$ is the transmissivity of M2.

According to the above analysis, it can be known that the current output signal is related to the past output signal. What is received by the receiver is the past signal that was reflected by the receiver and then experienced a series of transmission losses, the gain, and the intensity modulation in a circulation. According to this fact, we come out the demodulation method relying on not only the present signal but also the past signal just before a circulating period $n_c = 2(n_{\text{L}} + n_{\text{R}} + 1)$. This scheme can be expressed by a division, namely, the demodulated signal is obtained as

$$\begin{aligned} y[n] &= \frac{P_{\text{out}}[n]}{P_{\text{out}}[n - n_c]} \\ &= \Gamma_{\text{loss}}G[n]s[n - n_c/2], \end{aligned} \quad (23)$$

and

$$\Gamma_{\text{loss}} = R_{\text{M1,EOM}}\Gamma_{\text{L1}}^2\Gamma_{\text{g}}^2\Gamma_{\text{diff}}\Gamma_{\text{air}}^2\Gamma_{\text{L2}}^2R_{\text{M2}}, \quad (24)$$

where Γ_{loss} contains all the static loss factors in the cavity, and $G[n]$ represents the dynamic gain of the gain medium. n_c can be estimated by positioning technologies plus a signal processing method; we discuss this issue in the next Section. Note that we assume the loss is static, because its variation speed depends on the moving/rotating speed of receivers which is very slow compared with the modulation speed. For instance, the maximum moving speed of human is 44 m/s [8], we can derive that cutting off a beam with diameter of 1 mm needs at least 22.7 μs ; this is very long in contrast to the modulation period which is below 1 ns.

From (23), we can see that the demodulated signal consists of three parts, i.e., the static loss, the dynamic gain, and the control signal. Consequently, if we want to retrieve the EOM's control signal correctly, the variation speed of $G[n]$ should be as slow as possible. Since the gain (related to the stimulated emission term $N_2\varphi\sigma c$) depends on the excited atom density N_2 , we should ensure that the variation speed of N_2 is small compared with that of the photon density φ . Fortunately, this condition can be satisfied in the SSLR system under some specific conditions, as the gain medium can be viewed as a circuit with a capacitor (see Fig. 5 in [28]) which stores excited atoms and releases them with a relatively slow speed. For instance, assuming that the photon density

in the gain medium is $\varphi = 5.679339 \times 10^{16} \text{ m}^{-3}$ (i.e., the intra-cavity beam power is 10 W and the gain medium radius $a_{\text{g}} = 1 \text{ mm}$) and the pump power is 20 W, we can obtain that, at the stable state where $\partial N_2/\partial t = 0$, the excited atom density $N_2 = 1.181963 \times 10^{24} \text{ m}^{-3}$. Then, we assume a step change φ_{δ} is added to the photon density, i.e., φ becomes $\varphi + \varphi_{\delta}$. We can see that the instantaneous change rate of the atom density becomes

$$\frac{\partial N_2}{\partial t} = -5.531587 \times 10^{10} \times \varphi_{\delta}. \quad (25)$$

If we set $\varphi_{\delta} = -0.1\varphi$ and the duration $\Delta t = 20 \text{ ns}$ (one period for photons to oscillate inside a 3-m long resonator), we can obtain that the change of the atom density $\Delta N_2 = 6.283152 \times 10^{18}$, which is much less than N_2 . Thus, we can ignore the effect induced by the variation of N_2 . Intuitively, as demonstrated in Fig. 4, we can observe that the gain medium performs like a capacitor, and the step response time is almost at millisecond level, which is much longer than an information symbol. From the above analysis, we conclude that the gain of the gain medium $G[n]$ can be considered as a static value within a symbol duration under some specific parameter settings, and this is also verified by the simulation results presented in Section IV.

III. IMPLEMENTATION

As depicted in (15)–(19), the discrete rate equations provide the basic model for the time-domain simulation of the resonant beam system. In this section, we demonstrate using these equations to implement a simulation algorithm in Matlab/Simulink software. In the next section, we use this simulation program to give an insight into the fluctuation of the intra-cavity resonant beam power at several stages, including initiating resonance, being interrupted, and rebuilding resonance, which are inevitable processes in the resonant beam system. We also demonstrate how the intra-cavity echo interference arises when the resonant beam is modulated, and especially, verify the feasibility of the proposed delay-divide demodulation method.

A. SSLR Simulation

As depicted in Fig. 5, the simulation system contains four parts, i.e., the transmitter, the free space, the receiver, and the demodulation module. Between any two optical devices, there is a delay model on each transmission line to model the beam transfer delay. Each optical device is represented by a customized Simulink model. Since this program only considers the intra-cavity power circulation without investigating the geometry of the beam, those passive elements such as the lenses, the mirrors, the air loss, and the splitter can be easily modeled by the gain model originally provided by Simulink. The most significant model created by us is the gain medium model which has four ports for the input and output of the traveling beams at opposite directions. The gain medium model simulates the dynamic behavior of the excited atom density N_2 and the photon density amplification as the beam passes, based on the discrete rate equations in (15)–(17), as demonstrated in Fig. 6. The quantity in the circulation is the

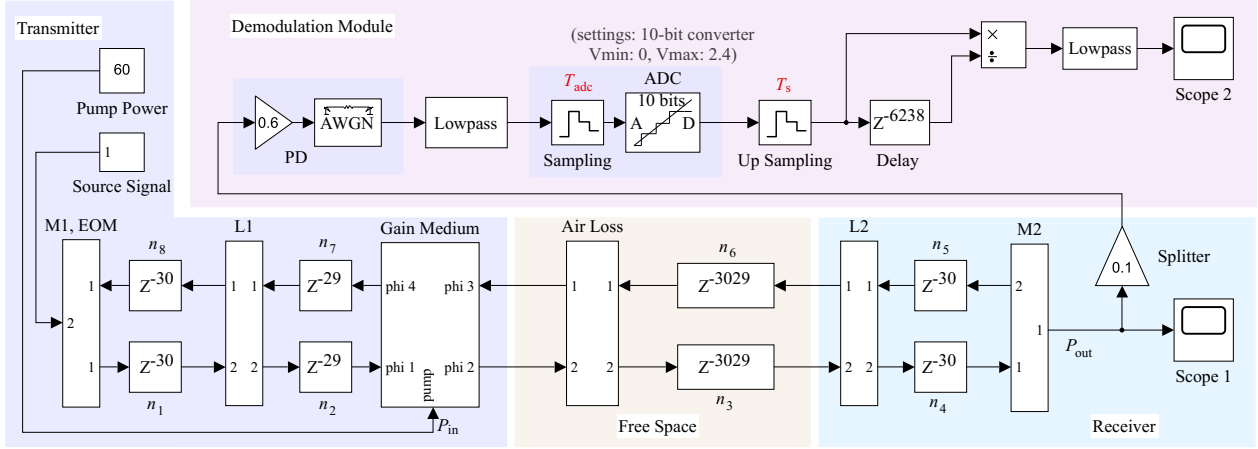


Fig. 5. Simulation system implemented in the Simulink environment

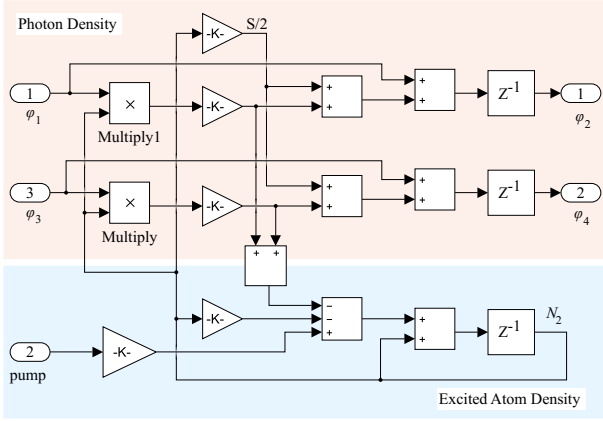


Fig. 6. The gain medium model

beam power, while the quantity computed in the gain medium model is the photon density; they have different units. Hence, a conversion/inversion between these two quantities should be added to the input/output ports of the gain medium model, using the relation expressed in (21).

The simulation accuracy is determined by the length of time step and the optical gain of the gain medium. The discretization process may result in an incorrect decrease of the optical gain. To increase the accuracy, the gain medium is divided into 10 slices, as depicted in Fig. 7. Here, each slice has the same implementation with the gain medium model depicted in Fig. 6. The pump source power P_{in} is also divided equally into 10 parts; and each part is sent into a slice. This cascade model can well simulate the gradient of the gain value inside the gain medium, which greatly increases the simulation accuracy. Note that, before entering the cascade model, the input signal is upsampled with a faster period ($T_s/10$) than the original sample period T_s to meet the time step requirement of each slice. After going out of the cascade model, the output signal is downsampled with the original period T_s to speed up the simulation. The parameters involved in simulation are listed in Table I. Besides, we set $R_{M1,EOM} = 98.5\%$, $\{\Gamma_{L1}, \Gamma_{L2}, \Gamma_g\} = 99\%$. The air loss Γ_{air}

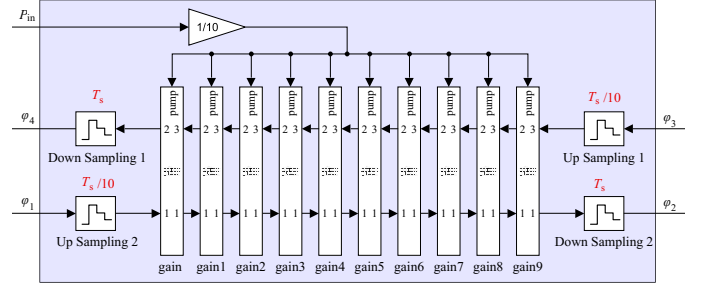


Fig. 7. The gain medium model consists of several thinner slices

and the diffraction loss Γ_{diff} are very small at $d = 3$ m, which can be obtained according to [34] and [17], respectively. The output resonant beam power waveform can be observed by Scope 1. In this paper, unless otherwise specified, the pump source power P_{in} and the output mirror reflectivity R_{M2} are set to 60 W and 90%, respectively. As shown in Fig. 8, the stable-state output optical powers from the simulation results under different parameter settings are in good agreement with the theoretical results computed by the closed-form formula expressed in (6)–(8).

B. Delay-Divide Demodulation Module

We also implement the delay-divide demodulation method in the simulation program. Here, we set the splitting ratio of optical power for demodulation is $r = 0.1$. The PD's responsivity, which converts the optical power into current, is $\rho = 0.6$ A/W. We assume the load resistor of the PD is 1Ω , so that the output voltage is equal to the current. Both the splitter and the PD can be expressed by Simulink gain models. Since the EOM performs like a multiplier, the circulating signal inside the cavity will be moved to very-high frequency band by modulation process. However, the variation imposed on the intra-cavity signal within one round-trip does not exceed the frequency of the source signal. This condition gives us the opportunity of using a lowpass filter (LPF) to filter out the useless frequencies and meanwhile

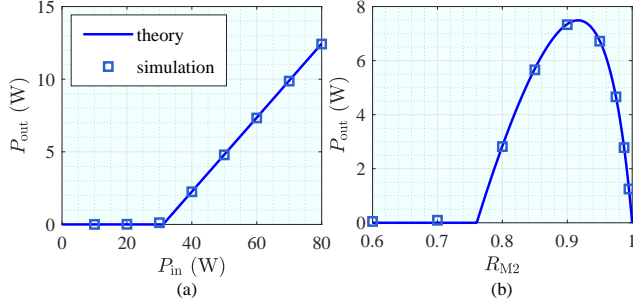


Fig. 8. Comparison of stable-state output power P_{out} between simulation and theoretical computation under (a) different pump source power P_{in} and (b) different output mirror reflectivity R_{M2}

preserve the important information. Hence, the first LPF in the demodulation module is employed to remove the high-frequency components from the received signal. Next, the down sampling with period of T_{adc} models the sampling process of the analog-to-digital converter (ADC), as the ADC model here operates continuously. The sample rate should be set large enough to prevent distortion of the passing signal, and we will investigate this issues in the next section. In Fig. 5, the ADC resolution is set to 10 bits. The maximum input of the ADC is limited to be no greater than 2.5 V.

After the conversion of ADC, the signal is stored in the memory as bits. Then, an upsampling model which can be realized by a digital processor in practice is placed on the line for accurate alignment. Next, a copy of the signal is sent to a delay model, which can be realized by a first input first output (FIFO) memory. The current signal is divided by the past signal received just before a delay time. This computes the variation of the intra-cavity loss and the gain within a round-trip, as verified by (23). Hence, the delay time equals one period of circulation of the intra-cavity beam, i.e., it depends on the transmission distance. We can use positioning/ranging method to obtain the distance in rough and then use the signal processor to find the accurate delay time. If the delay time is correct, the BER reaches the minimum value. The processed signal is then sent to the second LPF to remove any undesired frequencies generated from the division operation. Finally, on the output port of the second LPF, we can observe the demodulated signal by Scope 2. In the next section, we study the performance of the proposed demodulation method.

IV. RESULTS

Now, we are able to use time-domain simulations to observe the variation of the resonant beam power in a very small timescale under a very fast modulation frequency. We first observe the dynamic process when the resonance is initiated. Then, we observe the responses when foreign objects is inserted into the cavity and when the intra-cavity modulation is conducted. Next, we study the spectrum of the gain variation of the gain medium to clarify the reason of the question: Why does the proposed delay-divided demodulation scheme work? Finally, we obtain the BER of the proposed system and

TABLE I
SYSTEM PARAMETERS [31, 35]

Parameter	Symbol	Value
Saturation intensity	I_s	$1.1976 \times 10^7 \text{ W/m}^2$
Stimulated emission cross section	σ	$15.6 \times 10^{-23} \text{ m}^2$
Fluorescence lifetime	τ_f	100 μs
Decay time from E_2 to E_1	τ_{21}	115 μs
Resonant beam wavelength	λ	1064 nm
Combined pumping efficiency	η_c	43.9%
Spontaneous emission factor	β	0.001
Gain medium radius	a_g	2 mm
Gain medium thickness	l_g	1 mm
Combined pumping efficiency	η_c	43.9%
Focal length of lens	f	30 mm
Mirror-to-lens interval	l	30.225 mm
Transmission distance	d	3 m
DC bias	p	0.98 V
Splitting ratio	r	0.1
PD's responsivity	γ	0.6 A/W

demonstrate the effects induced by the sample rate and the resolution of the ADC.

A. Initiating Resonance

As the pump power starts to input the gain medium, the excited atom density increases rapidly, so the gain of the gain medium is very high. Then, the resonant beam experiences a period of variation called *relaxation oscillation*. As shown in Fig. 9, at the beginning of the relaxation oscillation, the resonant beam power is quickly amplified to a very high level by stimulated emission. However, the excited atoms are also consumed during the stimulated emission process, and the decrease rate of the excited atom density raises with the increase of the resonant beam power. The resonant beam power then starts to decrease and quickly drops to a very low level, since the excited atoms are largely consumed. The above oscillation repeats with a decay and reaches a stable state after several oscillation periods.

Fig. 9 depicts the output optical power P_{out} in time-domain under different pump power P_{in} . We can observe that with higher P_{in} , the resonant beam experiences more severe relaxation oscillation. The oscillation frequency, the start-up time, and the peak power increases with the growth of P_{in} . Fig. 10 demonstrates the relaxation oscillation under different output mirror reflectivity R_{M2} . We can see that higher R_{M2} leads to more violent relaxation oscillation. Although the peak output power under $R_{M2} = 0.995$ looks very low, the resonant beam power inside the cavity is very high, as most power is reflected back to the cavity by the mirror M2. From another perspective, we can compare the peak beam power with the beam power at the stable state and then find that under $R_{M2} = 0.995$ the relaxation oscillation is quite serious. We also find that the relaxation oscillation lasts for less than 0.5 ms and the frequency is around 50 kHz under the given parameter setting.

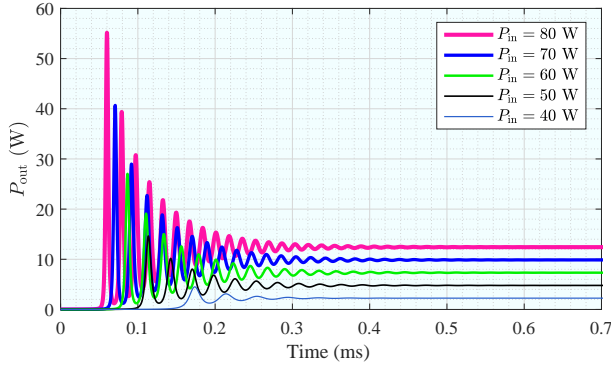


Fig. 9. Relaxation oscillation under different pump source power P_{in}

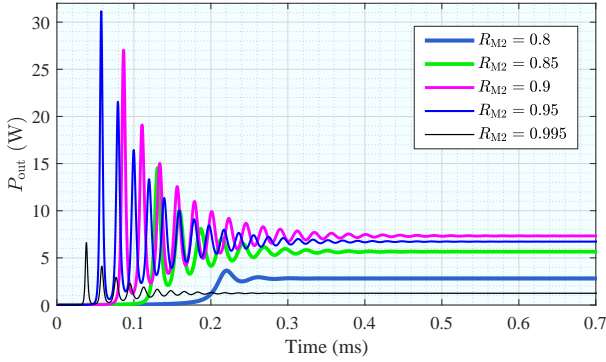


Fig. 10. Relaxation oscillation under different output mirror reflectivity R_{M2}

B. Response to Invasion and Modulation

Now, we study the response of the output beam power when an external influence is applied to the resonant beam. The most common case is that a foreign body is inserted into the cavity. The action of intrusion can be modeled as a continuing change of the intra-cavity diffraction loss. In simulation, we add a transmissivity on the intra-cavity beam path to perform this action. The transmissivity decreases from 1 to 0 within $22.7 \mu\text{s}$ (referring to the aforementioned maximum moving speed of human body) and then raises to 1 again after a period of time. As shown in Fig. 11, the resonance ceases quickly as the foreign object invades the cavity. As the object leaves, the resonance restarts with the occurrence of relaxation oscillation. Different from the first initiation caused by the start-up of the pump source, the leaving of the foreign object causes a narrow pulse whose power is up to 1493 W. This phenomenon arises from the retention of the excited atoms at the upper energy level E_2 , as there is no photon contributing to the transition of the excited atoms when the beam path is obstructed. The optical gain provided by the gain medium becomes very high with the increase of the excited atom density. As the object leaves, the extremely high gain leads to the high-power pulse; and then, the excited atoms exhaust quickly, leading to the transient pulse duration. Because most of the excited atoms are consumed by the pulse, the subsequent relaxation oscillation pattern is similar to the first one. Since the pulse width is very small, it is unnecessary to concern the safety of the receiving devices.

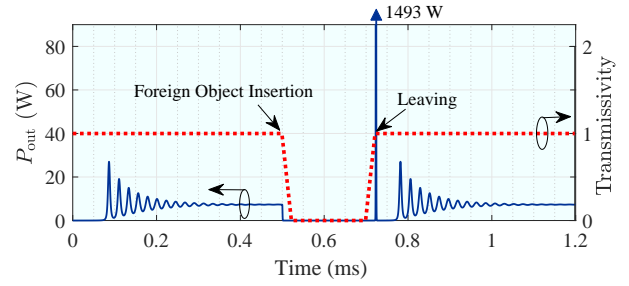


Fig. 11. Output power response to foreign object invasion

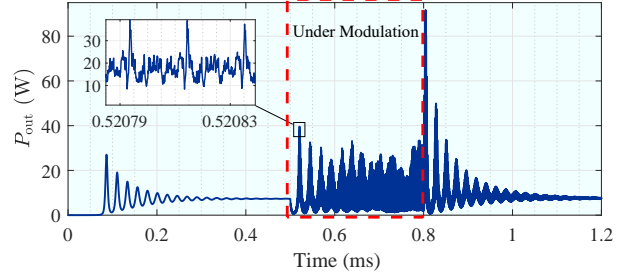


Fig. 12. Output power response to modulation and terminating modulation

In Fig 12, we demonstrate the output power response to the modulation (1-Gbit/s on-off keying signal with a DC bias) conducted by the EOM. It can be observed that the beam power starts to fluctuate as the modulation is conducted. It can be found that the variation of the output power is the superposition of a fast fluctuation and a slow fluctuation (see the envelope). The fast fluctuation is caused by the modulation, although we cannot directly recognize the source signal from the wave. The slow fluctuation comes from the loss of balance of the resonant system which happens when the loss or the input power is changed. Here, the change of the total loss is induced by modulation, since the EOM changes its transmissivity during modulation. As the modulation stops, we can also observe a short pulse which is similar to Fig. 11. This phenomenon has the same reason with the leaving process of a foreign object, as the termination of the modulation reduces the intra-cavity loss suddenly. The subsequent process is also similar to Fig. 11, but we can see that the fast fluctuation continues. The fast fluctuation after terminating the modulation comes from the circular transfer of the intra-cavity beam (the reason of echo interference). Nevertheless, without modulation, the fast fluctuation exhibits a decay as time goes on.

C. Demodulation

From Fig. 12, we can find that it is quite difficult to retrieve the source information from such a chaotic output. Fortunately, the slow variation speed of the gain of the gain medium provides the opportunity of demodulating the signal. We have put forward the delay-divide demodulation method in Section II.C. Now, we exploit simulation to observe the spectrum of the gain variation and then find if the requirement of demodulation can be met. The waveform of the gain is

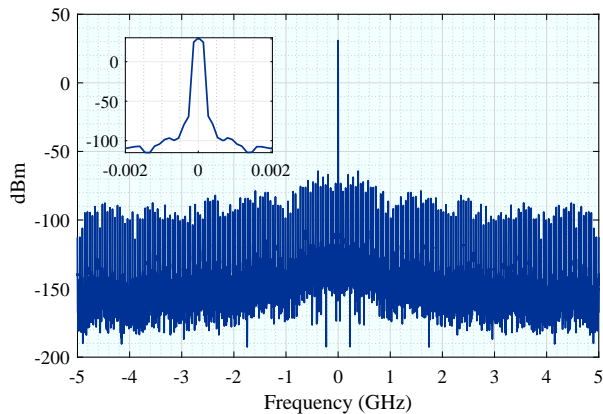


Fig. 13. Spectrum of the gain fluctuation of the gain medium

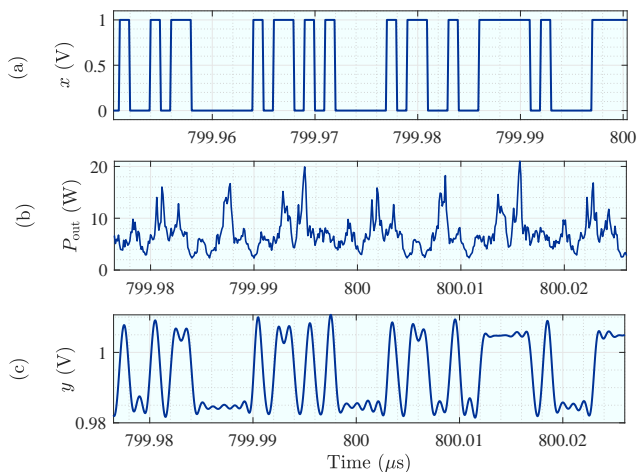


Fig. 14. Demonstration of demodulation: (a) the source signal; (b) the output signal at mirror M₂; and (c) the demodulated signal

obtained by computing the ratio of the output power from the gain medium model to the input which was recorded (using a delay model) just when the photon entering the gain medium. We calculated the spectrum of the gain waveform, as depicted in Fig. 13. It can be found that the significant frequency of the gain waveform is less than 250 kHz, which is much smaller than the modulation frequency. As demonstrated in (23), the demodulation is just realized by computing the round-trip change (induced by the gain and the total loss) of the intra-cavity resonant beam power. So far, we have found that both the gain and the loss can be viewed as static values in small timescale. The slow change of the gain in large timescale can be overcome by using training sequence which is a common method in wireless communications. Fig. 14 demonstrates an example of modulation and demodulation. It is easy to find that the demodulated signal in Fig. 14(c) matches the source signal in Fig. 14(a) well, although the variation of the output power in Fig. 14(b) looks chaotic.

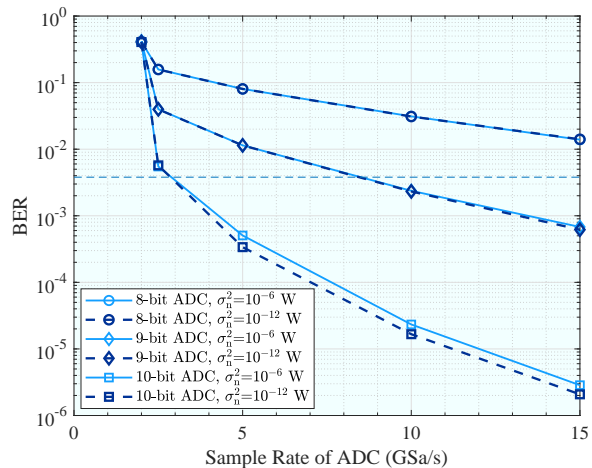


Fig. 15. Bit error rate vs. ADC sample rate under different ADC resolution bits and noise variance σ_n^2

D. Bit Error Rate

We conduct a communication simulation to evaluate the performance of the proposed demodulation method. The source signal is 1-Gbit/s binary data. Thus, the passband edge frequency and the stopband edge frequency of each LPF are set to 1 GHz and 1.2 GHz, respectively. The source signal is added to a DC bias, forming the control signal of the EOM. The bias $p = 0.98$ V, and thus, the amplitude of source is limited to be 0.02 V. We assume the conversion from the control signal to the EOM's transmissivity is not scaled. The pump power P_{in} is set to 60 W. Referring to Fig. 8(b), we choose $R_{M2} = 90\%$ to obtain a high output power as possible. The modulation is initiated 0.5 ms after the pump source being turned on. The demodulated waveform is then sampled with the same rate of the source symbol, but a phase offset is applied to this sampling operation to meet the best sampling position. These samples is split into several segments, and each segment contains 500 samples. These segments are processed independently to overcome the slow fluctuation of the gain. The zero-one determination threshold for the samples in a segment is the average value of these samples. BER is counted for evaluating the communication performance. We examine several factors that may affect the performance, including the ADC's sample rate, the ADC's resolution bits, and the noise level. As demonstrated in Fig. 15, with the increase of the ADC's sample rate, the BER decreases relatively. ADC with 10-bit resolution provides better performance than that with 8-bit resolution. Due to the high power of the receiving signal, the noise exhibits less effect on the performance. We can see that most simulation cases can achieve $BER > 3.8 \times 10^{-3}$ (the threshold of 7% hard-decision forward error correction [36]) when the ADC has 10-bit resolution. This result shows that it is feasible to extract the source signal directly from the waveform of the resonant beam power without any complex modulation schemes and redundant optical devices.

V. CONCLUSIONS

In this paper, a time-domain simulation algorithm for the resonant beam charging and communication system and a delay-divide demodulation method are proposed. The simulation algorithm can monitor the variation of every dynamic parameter in the resonant beam system with a very small timescale which is even less than the time for photons to pass through an optical device. Also, the system response to the fast modulation applied to the intra-cavity beam can also be monitored by the simulation algorithm. We compared the simulation results at the final stable state with the theoretical computation, verifying the high accuracy of the simulation algorithm. Using the simulation algorithm, we observed the system response to four important actions, including the start-up of pumping, the invasion and leaving of foreign objects, and the intra-cavity modulation. By observing the spectrum of the gain fluctuation waveform, we found that the frequency of the gain fluctuation is much smaller than the modulation frequency, verifying that the required condition of the proposed demodulation method is satisfied. The demodulation method is also realized in the simulation system. We conducted on-off keying modulation and count the bit error rate to demonstrate the communication performance, which also verify the feasibility of extracting the source information directly from the chaotic waveform of the received resonant beam power.

REFERENCES

- [1] J. D. N. Dionisio, W. G. Burns III, and R. Gilbert, "3D virtual worlds and the metaverse: Current status and future possibilities," *ACM Comput. Surv.*, vol. 45, no. 3, pp. 1–38, July 2013.
- [2] Z. Fei, F. Wang, J. Wang, and X. Xie, "QoE evaluation methods for 360-degree VR video transmission," *IEEE J. Sel. Topics Signal Process.*, vol. 14, no. 1, pp. 78–88, Jan. 2020.
- [3] K. Oiwake, K. Komiya, H. Akasaki, and T. Nakajima, "VR classroom: Enhancing learning experience with virtual class rooms," in *Eleventh International Conference on Mobile Computing and Ubiquitous Network (ICMU)*, Auckland, New Zealand, Oct. 2018, pp. 1–6.
- [4] K. David and H. Berndt, "6G vision and requirements: Is there any need for beyond 5G?" *IEEE Veh. Technol. Mag.*, vol. 13, no. 3, pp. 72–80, July 2018.
- [5] Q. Liu, J. Wu, P. Xia, S. Zhao, W. Chen, Y. Yang, and L. Hanzo, "Charging unplugged: Will distributed laser charging for mobile wireless power transfer work?" *IEEE Veh. Technol. Mag.*, vol. 11, no. 4, pp. 36–45, Nov. 2016.
- [6] M. Xiong, Q. Liu, M. Liu, X. Wang, and H. Deng, "Resonant beam communications with photovoltaic receiver for optical data and power transfer," *IEEE Trans. Commun.*, vol. 68, no. 5, pp. 3033–3041, May 2020.
- [7] M. Xiong, Q. Liu, G. Wang, G. B. Giannakis, and C. Huang, "Resonant beam communications: Principles and designs," *IEEE Commun. Mag.*, vol. 57, no. 10, pp. 34–39, Oct. 2019.
- [8] V. Iyer, E. Bayati, R. Nandakumar, A. Majumdar, and S. Gollakota, "Charging a smartphone across a room using lasers," *Proc. ACM Interact. Mob. Wearable Ubiquitous Technol.*, vol. 1, no. 4, pp. 1–21, Jan. 2017.
- [9] T. Koonen, A. Khalid, J. Oh, F. Gomez-Agis, and E. Tangdionga, "High-capacity optical wireless communication using 2-dimensional IR beam steering," in *Opto-Electronics and Communications Conference (OECC) and Photonics Global Conference (PGC)*, Singapore, Nov. 2017, pp. 1–4.
- [10] T. Koonen, J. Oh, K. Mekonnen, and E. Tangdionga, "Ultra-high capacity indoor optical wireless communication using steered pencil beams," in *Proc. International Topical Meeting on Microwave Photonics*, Paphos, Cyprus, Oct. 2015, pp. 4802–4809.
- [11] H. Rhee, J. You, H. Yoon, K. Han, M. Kim, B. G. Lee, S. Kim, and H. Park, "32 Gbps data transmission with 2D beam-steering using a silicon optical phased array," *IEEE Photon. Technol. Lett.*, vol. 32, no. 13, pp. 803–806, May 2020.
- [12] Z. Zhang, J. Dang, L. Wu, H. Wang, J. Xia, W. Lei, J. Wang, and X. You, "Optical mobile communications: Principles, implementation, and performance analysis," *IEEE Trans. Vehi. Technol.*, vol. 68, no. 1, pp. 471–482, Nov. 2019.
- [13] C. E. O’Lone, H. S. Dhillon, and R. Michael Buehrer, "Characterizing the first-arriving multipath component in 5G millimeter wave networks: TOA, AOA, and non-line-of-sight bias," *IEEE Trans. Wireless Commun.*, 2021, to appear, doi:10.1109/TWC.2021.3105641.
- [14] G. J. Linford, E. R. Peressini, W. R. Sooy, and M. L. Spaeth, "Very long lasers," *Appl. Opt.*, vol. 13, no. 2, pp. 379–390, Feb. 1974.
- [15] G. J. Linford and L. W. Hill, "Nd:YAG long lasers," *Appl. Opt.*, vol. 13, no. 6, pp. 1387–1394, June 1974.
- [16] R. Della-Pergola, O. Alpert, O. NAHMIAS, and V. Vaisleib, "Spatially distributed laser resonator," Worldwide Patent WO2012172541A1, Dec. 20, 2012.
- [17] M. Xiong, M. Liu, Q. Jiang, J. Zhou, Q. Liu, and H. Deng, "Retro-reflective beam communications with spatially separated laser resonator," *IEEE Trans. Wireless Commun.*, vol. 20, no. 8, pp. 4917–4928, Aug. 2021.
- [18] Q. Liu, M. Xiong, M. Liu, Q. Jiang, W. Fang, and Y. Bai, "Mobile wireless power transfer using a self-aligned resonant beam," *arXiv preprint arXiv:2105.13174*, 2021.
- [19] W. Wang, Y. Gao, D. Sun, X. Du, J. Guo, and X. Liang, "Adjustable-free and movable Nd:YVO₄ thin disk laser based on the telecentric cat’s eye cavity," *Chin. Opt. Lett.*, vol. 19, no. 11, p. 111403, Aug. 2021.
- [20] W. Fang, H. Deng, Q. Liu, M. Liu, Q. Jiang, L. Yang, and G. B. Giannakis, "Safety analysis of long-range and high-power wireless power transfer using resonant beam," *IEEE Trans. Signal Process.*, vol. 69, pp. 2833–2843, May 2021.
- [21] M. Liu, M. Xiong, Q. Liu, S. Zhou, and H. Deng, "Mobility-enhanced simultaneous lightwave information and power transfer," *IEEE Trans. Wireless Commun.*, vol. 20, no. 10, Oct. 2021.
- [22] J. Lim, T. S. Khwaja, and J. Ha, "Wireless optical power transfer system by spatial wavelength division and distributed laser cavity resonance," *Opt. Express*, vol. 27, no. 12, pp. A924–A935, June 2019.
- [23] D. Li, Y. Tian, and C. Huang, "Capacity analysis of mobile resonant beam communications," in *IEEE International Conference on Communications (ICC)*, 2021, to appear, doi:10.1109/ICC42927.2021.9500944.
- [24] M. Xiong, Q. Liu, G. Wang, G. B. Giannakis, S. Zhang, J. Zhu, and C. Huang, "Resonant beam communications with echo interference elimination," *IEEE Internet Things J.*, vol. 8, no. 4, pp. 2875–2885, Feb. 2021.
- [25] M. Xiong, Q. Liu, X. Wang, S. Zhou, B. Zhou, and Z. Bu, "Mobile optical communications using second harmonic of intra-cavity laser," *arXiv preprint arXiv:2106.11116*, 2021.
- [26] R. Mys, "Time dependent simulation of laser by Gauss-modes," Master’s thesis, Friedrich Alexander University Erlangen-Nuremberg, Sept. 2005.
- [27] T. Schaer, R. Rusnov, S. Eagle, J. Jastrebski, S. Albanese, and X. Fernando, "A dynamic simulation model for semiconductor laser diodes," in *Canadian Conference on Electrical and Computer Engineering. Toward a Caring and Humane Technology (Cat. No.03CH37436)*, May 2003, pp. 293–297.
- [28] J. Zhou, M. Xiong, M. Liu, Q. Liu, and S. Zhou, "Transient analysis for resonant beam charging and communication," *IEEE Internet Things J.*, 2021, to appear, doi:10.1109/JIOT.2021.3094809.

- [29] V. Magni, "Multielement stable resonators containing a variable lens," *J. Opt. Soc. Am. A*, vol. 4, no. 10, pp. 1962–1969, Oct. 1987.
- [30] N. Hodgson and H. Weber, *Laser Resonators and Beam Propagation: Fundamentals, Advanced Concepts and Applications 2nd ed.* New York, NY, U.S.: Springer, 2005.
- [31] W. Koechner, *Solid-State Laser Engineering, 6th ed.* New York, NY, USA: Springer, 2006.
- [32] M. Van Exter, G. Nienhuis, and J. Woerdman, "Two simple expressions for the spontaneous emission factor β ," *Phys. Rev., A*, vol. 54, no. 4, p. 3553, Oct. 1996.
- [33] L. Chen, B. Krongold, and J. Evans, "Theoretical characterization of nonlinear clipping effects in IM/DD optical OFDM systems," *IEEE Trans. Communi.*, vol. 60, no. 8, pp. 2304–2312, Aug. 2012.
- [34] I. I. Kim, B. McArthur, and E. J. Korevaar, "Comparison of laser beam propagation at 785 nm and 1550 nm in fog and haze for optical wireless communications," in *Proc. SPIE*, vol. 4214, no. 2, pp. 26–37, Feb. 2001.
- [35] W. Long, T. Wu, J. Jiao, M. Tang, and M. Xu, "Refraction-learning-based whale optimization algorithm for high-dimensional problems and parameter estimation of PV model," *Eng. Appl. Artif. Intell.*, vol. 89, p. 103457, Mar. 2020.
- [36] L.-Y. Wei, C.-W. Hsu, C.-W. Chow, and C.-H. Yeh, "20.231 Gbit/s tricolor red/green/blue laser diode based bidirectional signal remodulation visible-light communication system," *Photonics Res.*, vol. 6, no. 5, pp. 422–426, Apr. 2018.